metals

MDPI

Article

Comparison of the Internal Fatigue Crack Initiation and Propagation Behavior of a Quenched and Tempered Steel with and without a Thermomechanical Treatment

Amin Khayatzadeh *, Stefan Guth and Martin Heilmaier

Institute for Applied Materials (IAM-WK), Department of Mechanical Engineering, Karlsruhe Institute of Technology, Engelbert-Arnold-Str. 4, 76131 Karlsruhe, Germany; stefan.guth@kit.edu (S.G.); martin.heilmaier@kit.edu (M.H.)

* Correspondence: amin.khayatzadeh@kit.edu; Tel.: +49-721-608-44159

Abstract: Previous studies have shown that a thermomechanical treatment (TMT) consisting of cyclic plastic deformation in the temperature range of dynamic strain aging can increase the fatigue limit of quenched and tempered steels by strengthening the microstructure around non-metallic inclusions. This study considers the influence of a TMT on the shape, size and position of crack-initiating inclusions as well as on the internal crack propagation behavior. For this, high cycle fatigue tests on specimens with and without TMT were performed at room temperature at a constant stress amplitude. The TMT increased the average lifetime by about 40%, while there was no effect of the TMT on the form or size of critical inclusions. Surprisingly, no correlation between inclusion size and lifetime could be found for both specimen types. There is also no correlation between inclusion depth and lifetime, which means that the crack propagation stage covers only a small portion of the overall lifetime. The average depth of critical inclusions is considerably higher for TMT specimens indicating that the strengthening effect of the TMT is more pronounced for near-surface inclusions. Fisheye fracture surfaces around the critical inclusions could be found on all tested specimens. With increasing fisheye size, a transition from a smooth to a rather rough and wavy fracture surface could be observed for both specimen types.

Keywords: non-metallic inclusion; thermomechanical treatment (TMT); inclusion area; inclusion shape; inclusion depth; fisheye formation; crack initiation

Citation: Khayatzadeh, A.; Guth, S.; Heilmaier, M. Comparison of the Internal Fatigue Crack Initiation and Propagation Behavior of a Quenched and Tempered Steel with and without a Thermomechanical Treatment. *Metals* **2022**, *12*, 995. https://doi.org/10.3390/met12060995

Academic Editor: Francesco Iacoviello

Received: 12 May 2022
Accepted: 8 June 2022
Published: 10 June 2022

1. Introduction

Since fatigue crack initiation and growth is one of the significant causes of structural failure in engineering applications, there is a considerable demand for steels with high fatigue strength in the industry [1,2]. SAE4140 quenched and tempered steel is one of the most favorable steels for applications involving cyclic loading due to its high fatigue strength [3]. It is well-known that the lifetime of quenched and tempered steels in the high cycle fatigue (HCF) and very high cycle fatigue (VHCF) regimes are limited by crack initiation at internal inhomogeneities and non-metallic inclusions [4–7]. Normally, fracture surfaces of HCF and VHCF failures exhibit not only crack initiation at non-metallic inclusions but also fisheye formation around these critical inclusions [7,8]. Fisheye-forming cracks propagate in a vacuum until the free surface of the component or the specimen is reached and then surface crack propagation under the influence of the ambient atmosphere takes place [9]. The fisheye formation may take place in two stages forming a fine granular area (FGA) around the crack initiating inclusion and a neighboring smooth area (SA). Results of Stanzl-Tschegg et al. show that the smooth area of a fisheye may be followed by a rougher fracture surface indicating a more ductile fracture mode [10,11]. The crack propagation stage forming the rougher fracture surface was identified as the Paris regime [10]. However, it is noticeable that FGA formation may not necessarily be detectable for internal

crack initiation [12]. There are several studies about steel cleanliness and control of non-metallic inclusions to minimize the negative influence of critical inclusions and improve the fatigue strength [13,14]. In addition, the study of non-metallic inclusions, in particular with respect to their type, area, shape and position, is of high interest in order to predict the fatigue strengths of engineering steels and allow for safe design [1,15–19]. Besides approaches to enhance the purity of steels and minimizing critical inclusion formation during steel production, a thermomechanical treatment (TMT) in the temperature range of maximum dynamic strain aging (DSA) is another approach to increase the fatigue strength of steels by strengthening the microstructure around the inclusions after the steel production [20,21]. Increasing the fatigue limits of SAE4140 in the HCF and VHCF regimes by a TMT was recently shown in [22]. It is assumed that during the TMT, plastic deformation in the temperature range of DSA introduces a more stable dislocation structure around the non-metallic inclusions, which delays or prevents crack initiation thus resulting in higher HCF lifetimes and increased fatigue strengths [20]. However, the detailed mechanisms occurring in the vicinity of inclusions during a TMT are still unknown. Further, it is unclear whether the shape, area and position relative to the surface (e.g., depth) of an inclusion influence the effectiveness of a TMT or whether a TMT may affect the shape, area and position of critical crack-initiating inclusions. The shape, size and inclusion depth of crack-initiating non-metallic inclusions were investigated and analyzed by other researchers. However, these investigations are mostly simulation-based [15,23]. There are experimental investigations reporting no correlation between the areas of critical non-metallic inclusions or inclusion depth and lifetime (N_f) [9,24,25]. However, other studies showed that the area and inclusion depth of critical inclusions decreases with increasing lifetime [18,26]. In order to analyze the influence of non-metallic inclusions on the fatigue behavior, various parameters such as type, shape, area, distribution and applied stress should be taken into account and this makes the fatigue behavior analysis rather complex [17,27]. In this study, we systematically investigate the influence of shape, area and position of critical non-metallic inclusions on the high cycle fatigue lifetime of the steel SAE4140 in a quenched and tempered state. In a second step, we study whether a TMT, which increases the fatigue limit and the fatigue lifetime in the HCF regime [22], affects the shape, area and position of critical inclusions and whether the effectiveness of the TMT is influenced by these parameters. The goal of the study is to gain a better understanding of how the TMT and the inclusion parameters interact. For this, stress-controlled high cycle fatigue tests at room temperature were conducted on round specimens of quenched and tempered specimens and on additionally thermomechanically treated specimens of SAE4140. In order to rule out the influence of load amplitude, all fatigue tests were conducted with a constant stress amplitude. Fracture surfaces, fisheyes and inclusions were investigated using scanning electron microscopy (SEM) and energy dispersive X-ray spectroscopy (EDX).

2. Materials and Experimental Procedure

The investigated material is the steel SAE4140 (according to EN ISO 683-2, German designation: 42CrMo4) in quenched and tempered state. The chemical composition is given in Table 1. The material was delivered in soft-annealed state in the form of round bars from which a near-net-shape geometry of the specimens was machined by turning.

Table 1. Chemical composition of the test material in wt.%.

C	Si	Mn	P	S	Cr	Mo	Fe
0.430	0.259	0.743	0.012	0.039	1.060	0.207	Balance

After the quenching and tempering, the specimen geometries were again machined to avoid dimensional changes after heat treatment. The final specimen geometry for fatigue testing can be seen in Figure 1.

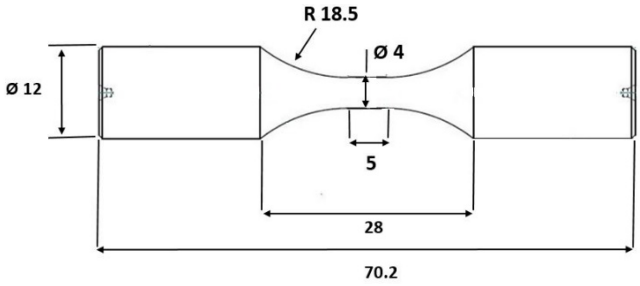

Figure 1. Specimen geometry used for experiments [28].

The initial heat treatment was conducted in a vacuum furnace and included austenitization at 840 °C for about 20 min, quenching in oil to reach room temperature and finally tempering at 180 °C for 2 h. After the heat treatment, a fully martensitic microstructure was obtained. In this state, the material exhibits a 0.2% yield strength of about 1500 MPa and ultimate tensile strength of 1900 MPa [29], which correlates to a hardness of 594 ± 5 HV 0.5. The hardness reduction due to the TMT, which takes place at 265 °C, is not significant [22]. The fatigue tests as well as the TMT were conducted on a servohydraulic push–pull testing machine with a capacity of 100 kN. The force was measured with a 100 kN force transducer. The TMT was conducted at a temperature of 265 °C, which was identified as temperature where the DSA effects are most pronounced [22]. The specimens were heated inductively to this temperature at zero stress and were kept in this state for 15 s soaking time. Then the cyclic mechanical treatment of the TMT was applied with a sinusoidal waveform at a frequency of 1 Hz and a gradually increasing stress amplitude according to the procedure described in [20]. The starting stress amplitude was 600 MPa and the maximum stress amplitude was 1600 MPa with a step of 100 MPa between individual stress amplitudes. At each stress amplitude, 5 cycles were applied. The total time of a specimen at 265 °C during the TMT was 70 s. A more detailed description of the TMT can be found in [22]. Specimens with thermomechanical treatment are designated as TMT specimens, while the specimens after the initial heat treatment served as a reference in the fatigue tests and are designated as heat treated (HT) specimens. Figure 2 shows micrographs of polished and etched longitudinal sections of an HT and a TMT specimen in the initial state. Both specimens exhibit a fully martensitic microstructure. There are no significant differences between HT and TMT specimens, which was expected since the annealing time of 70 s during the TMT at 265 °C is too short to cause changes that can be observed by light microscopy.

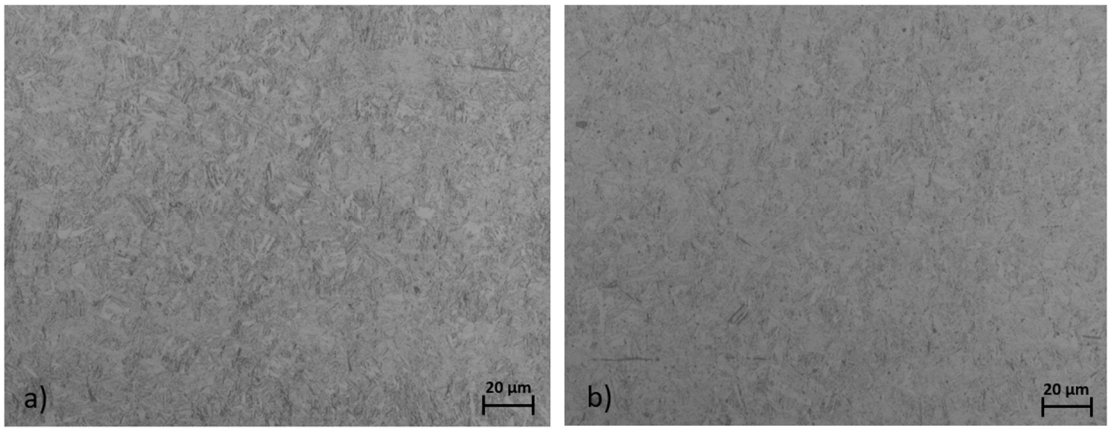

Figure 2. Representative light microscopic images of polished and etched longitudinal sections. The etchant was Nital. (**a**) HT specimen; (**b**) TMT specimen.

Both, TMT specimens and HT specimens were cycled in stress-controlled tests at room temperature until fracture. For cycling, a sinusoidal waveform with a frequency of 50 Hz was applied. The stress amplitude for all tests was 775 MPa with a load ratio of R = −1 (fully reversed loading). The stress amplitude of 775 MPa was chosen because it typically produces internal crack initiation at non-metallic inclusions as well as fisheye formation for both HT and TMT specimens [22]. The obtained lifetimes were between 1 and 10 million cycles. An SEM (Carl ZeissAG, Oberkochen, Germany) was used in secondary electron (SE) mode to analyze the fracture surfaces of specimens. The sizes and depths of inclusions and the sizes of fisheyes were measured using SEM images and the software KLONK image measurement (15.1.2.1, Image Measurement Corporation, Cheyenne, WY, USA). The inclusion depth was defined as minimum distance between the inclusion center and the surface. EDX (Thermo Fisher Scientific Inc., Waltham, MA, USA) was applied to determine the chemical composition of the non-metallic inclusions on fracture surfaces.

3. Results and Discussion

3.1. Lifetime Results

Figure 3 presents the fatigue lifetimes of all tested specimens (eight HT specimens and eight TMT specimens) at the constant stress amplitude of 775 MPa. In the considered lifetime regime, the TMT improved the average lifetime by about 40%, which is assumed to be a result of stabilization of the dislocation structure around inclusions and is consistent with the results of previous studies [21,22].

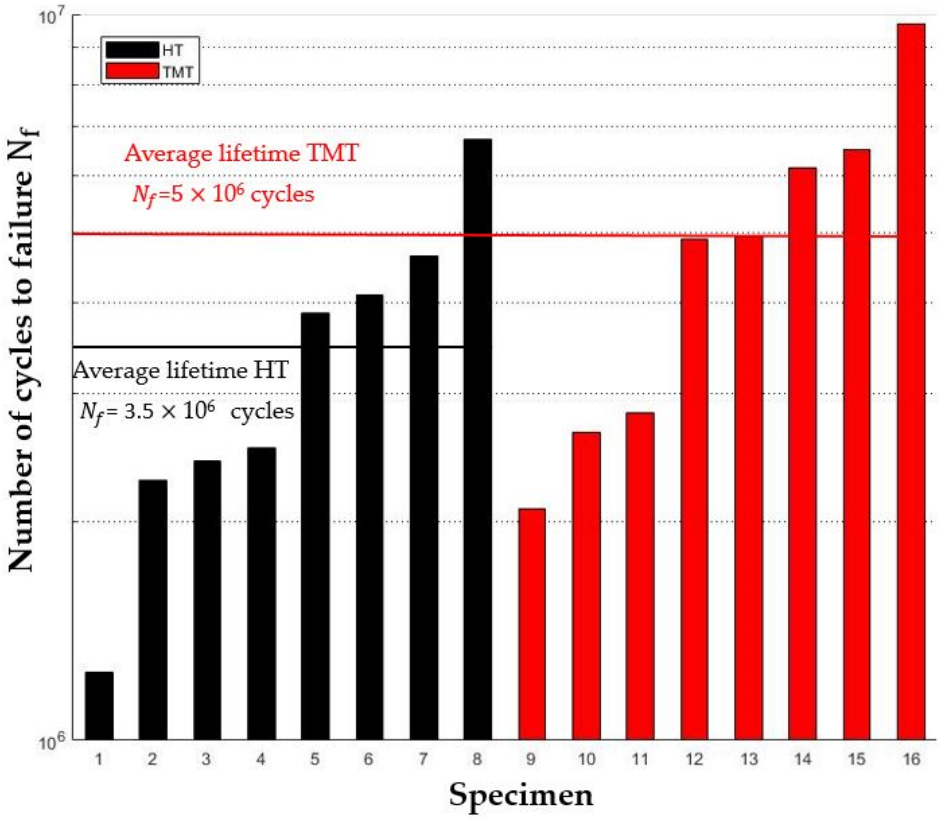

Figure 3. Fatigue lifetime analysis of HT and TMT specimens at given stress amplitude of 775 MPa.

3.2. Type and Form of Critical Non-Metallic Inclusions on the Fracture Surface

All tested specimens fractured due to cracks that initiated at inclusions in the volume. Chemical composition analysis using EDX showed that for both TMT and HT specimens the critical crack initiating inclusions were always oxides of type AlCaO. Figure 4 shows a representative SEM image of a crack-initiating inclusion along with the appropriate EDX mapping.

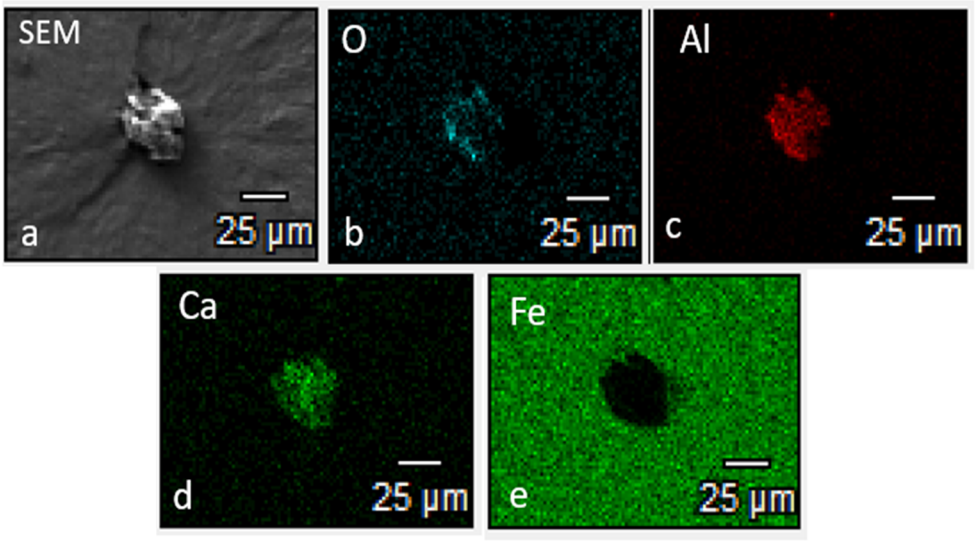

Figure 4. EDX mapping analysis of a crack-initiating inclusion. (**a**) SEM image; (**b**) O content; (**c**) Al content; (**d**) Ca content; (**e**) Fe content.

It was reported elsewhere that AlCaO oxides are typically the most harmful ones for internal fatigue crack initiation in SAE4140 [30]. Figure 5 shows typical critical inclusions on fracture surfaces. There are eye-shaped inclusions including sharp edges on one axis, which are produced during the rolling process [17], and round inclusions without sharp edges. Both forms of critical inclusions were found on the fracture surfaces of both the HT and TMT specimens.

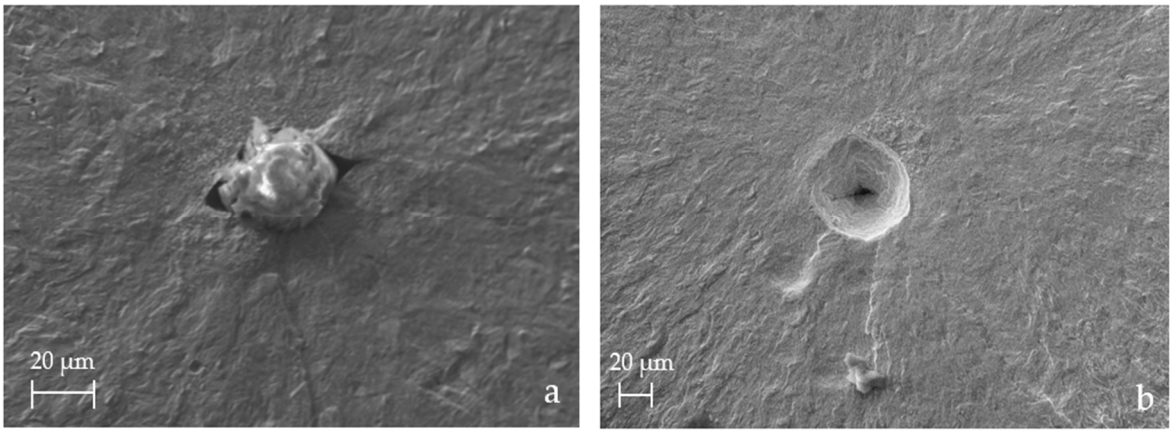

Figure 5. SEM images from two typical non-metallic inclusion shapes. (**a**) Eye-shaped inclusion with two sharp edges—HT specimen; (**b**) Round inclusion—TMT specimen.

Figure 6 shows two critical inclusions of TMT specimen fracture surfaces, which cannot be categorized into round or eye-shaped. Instead, these inclusions exhibit rather angular shapes, but without sharp edges. Nevertheless, also these inclusions were oxides of type AlCaO.

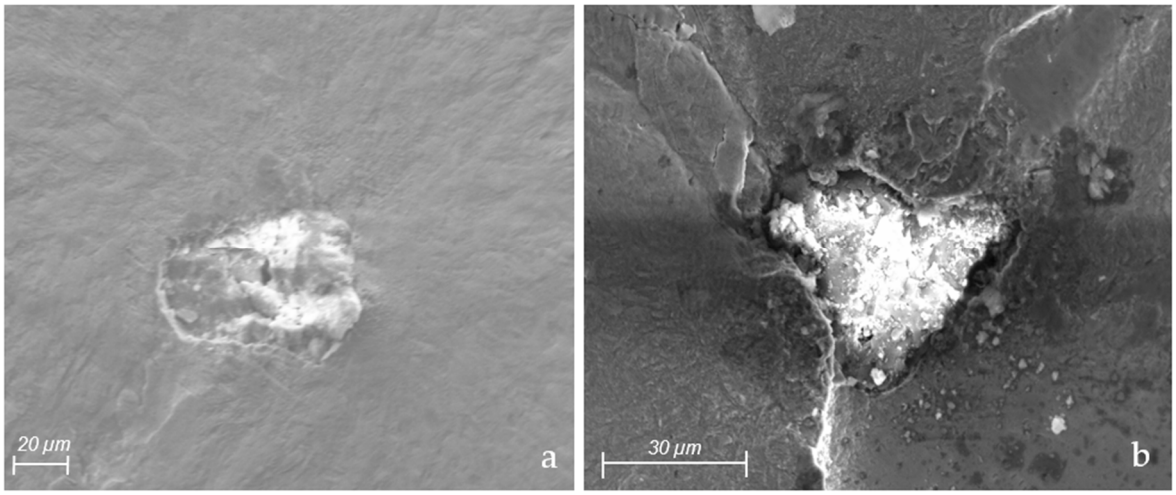

Figure 6. Critical inclusions. (**a**,**b**) with angular shape of TMT specimens.

3.3. Area, Shape and Maximum Stress Intensity Factor ($K_{max,Inc}$) of Non-Metallic Inclusion

Figure 7 shows the area of critical inclusions of TMT and HT specimens versus the fatigue lifetime for the constant stress amplitude of 775 MPa. The markers indicate the form of critical inclusion. For both HT and TMT specimens, the area of critical non-metallic inclusions scatters considerably. However, for both specimen types, no significant influence of the inclusion area on the lifetime can be observed. This is somewhat surprising since one might expect that for the given constant stress amplitude, larger inclusions lead to earlier crack initiation and thus shorter lifetimes. However, other studies have also shown that the HCF lifetime of steels after crack initiation at internal inclusions is independent of the inclusion area [9,24]. The average area of critical inclusions is slightly larger for TMT specimens than for HT specimens. Since the TMT has no influence on the inclusion size distribution, this slight effect is presumably due to the scatter of the inclusion sizes in the specimens. It can be seen that all round and angular-shaped critical inclusions for both HT and TMT specimens exhibit a square root area greater than about 35 µm. All critical inclusions with square root areas smaller than about 35 µm are eye-shaped with sharp edges. Hence, smaller inclusions with sharp edges can be as detrimental as larger ones without sharp edges, which can be explained by the stress concentration near the sharp edges [15,16]. Therefore, the area of inclusion is not the only significant parameter, which determines whether it can become a critical crack initiating inclusion.

With the measured area of the crack-initiating inclusions, the maximum stress intensity factor for subsurface inclusions can be derived with the following Equation (1):

$$K_{max,Inc} = 0.5 \times \sigma_{max} \times \sqrt{\pi \times \sqrt{area_{inc}}} \quad (1)$$

For a square root of the inclusion area of 35 µm, $K_{max,\,Inc}$ is about 4.05 MPa.$m^{1/2}$, which is apparently the required minimum to induce a fatigue crack from inclusions without sharp edges. For eye-shaped inclusions featuring sharp edges, the required value of $K_{max,\,Inc}$ is accordingly lower.

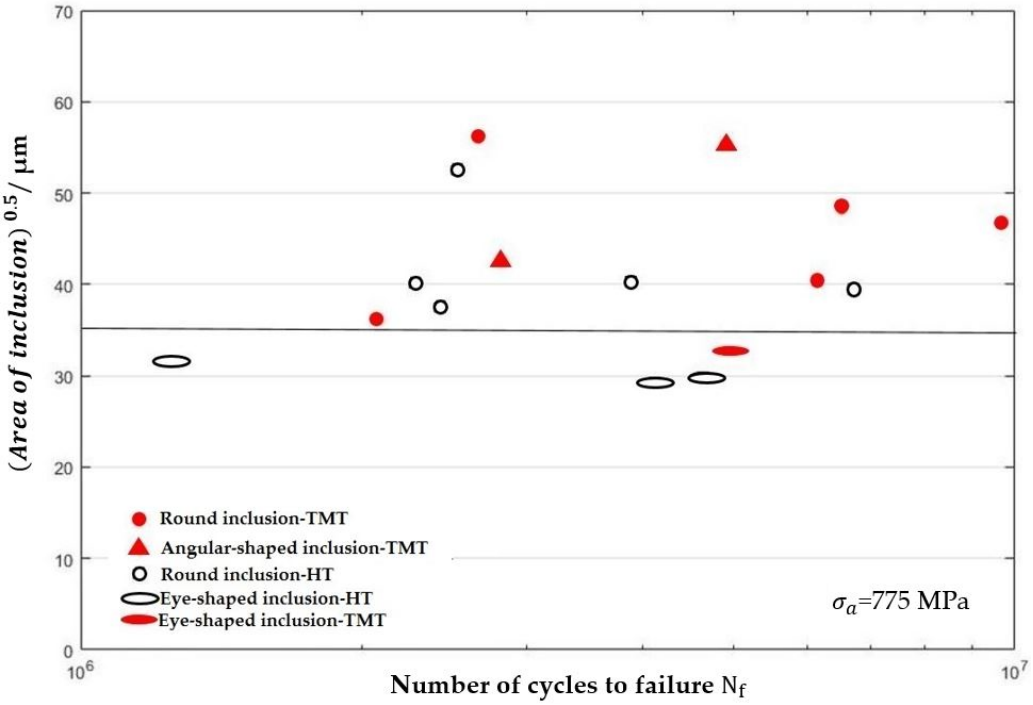

Figure 7. Area of critical inclusions for specimens with TMT and HT versus lifetime at σ_a = 775 MPa.

3.4. Influence of Inclusion Depth on the Fatigue Lifetime

Figure 8 compares the lifetimes of three HT specimens, which initiated cracks at inclusions of a similar size and form, but at various distances from the surface (inclusion depth). Apparently, the inclusion depth does not correlate with the lifetime. It can be assumed that due to the detrimental effect of air moisture, the crack propagation rate is much higher for an internal crack that has reached the surface than for a crack that is still in the fisheye stadium [11]. Consequently, the lifetime period spent in the crack propagation stage should be longer when the critical inclusion is located at a larger distance from the surface. Since the results indicate no obvious influence of inclusion depth which is in good agreement with other investigations in the HCF regime [24,25], we can infer that the lifetime is mostly governed by the period before crack initiation and the crack propagation stage occupies only a small percentage of the total lifetime. We assume that this is true for both HT and TMT specimens. Hence, the observed longer lifetimes for TMT specimens (see Figure 3) result presumably from longer periods until crack initiation, which is in accordance with the assumed TMT strengthening mechanism of a more stable dislocation structure around the inclusions. The parameter, which causes a lifetime scatter of about factor three for critical inclusions with almost the same size and form under constant stress amplitude and the same specimen state (Figure 8), remains unclear.

3.5. Fisheye Formation and Inclusion Depth

Fracture surface analyses of both TMT and HT specimens show the formation of fisheyes around all the critical inclusions. Figure 9 shows typical fracture surfaces of three specimens. As it can be seen from Figure 9a,b, cracks initiate at the inclusion inside the volume and the inclusion is surrounded by the fisheye. Both fisheyes exhibit a smooth area (SA) until reaching the surface and no obvious changes in the fisheye surface structure can be observed. As soon as the fisheye reaches the surface, oxidation-assisted fatigue crack growth begins. In this stage, the cracks grow predominantly away from the touching surface, as can be seen in Figure 9c. Hence, the formation of the nearly round fisheye ends as soon as the internal crack reaches the surface. The fisheye presented in Figure 9c shows a transition from smooth (SA) to rougher (RA) fracture surface with a wavy structure of radially extended peaks and troughs. A similar transition of the fisheye surface characteristics

was reported by Stanzl-Tschegg et al. [10,11] who found that the transition from smooth to rough fisheye surface goes along with a significant increase in crack propagation rate [11].

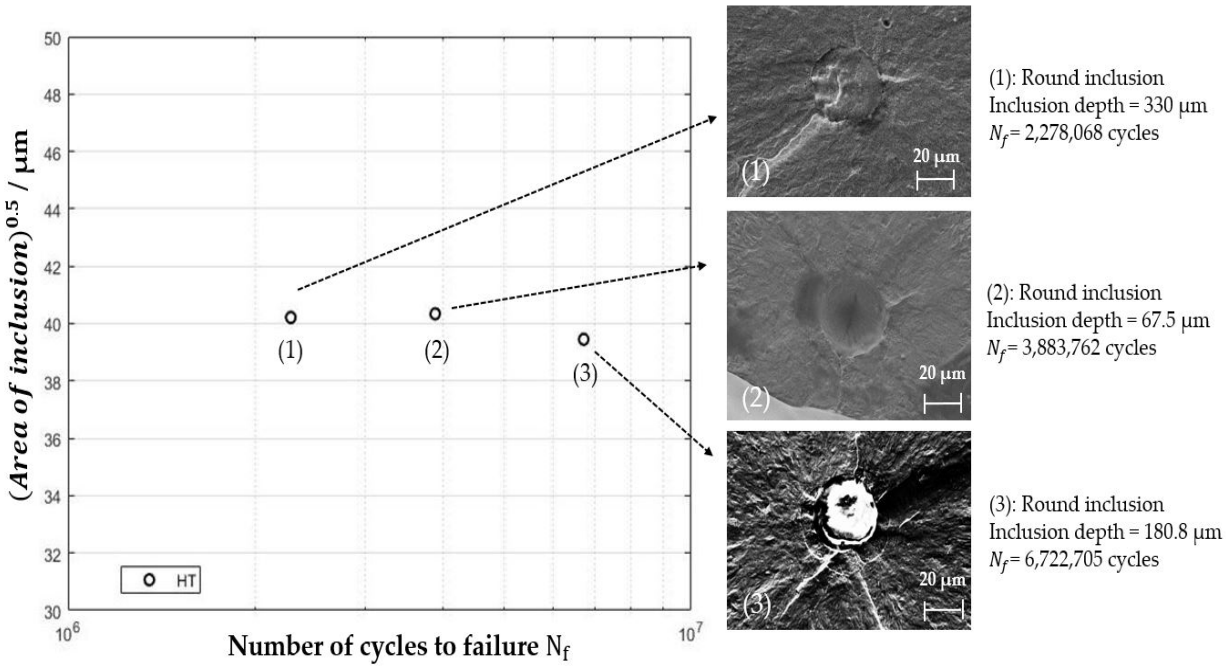

Figure 8. Evaluating the effect of inclusion depth on the lifetime for HT specimens at σ_a = 775 MPa.

Figure 10a,b show the fisheye radius and the inclusion depth over the fatigue lifetime, respectively. The data points in both diagrams correlate strongly, which confirms that fisheyes grow in circular form starting from the critical inclusion until they reach the surface. For both TMT and HT specimens there is no clear relation between inclusion depth or fisheye radius and lifetime. As already discussed in Section 3.4, this means that the lifetime portion in the crack propagation stage is relatively small. The fisheye sizes and the corresponding inclusion depths of TMT specimens are significantly larger than for HT specimens. This indicates that the TMT has a better strengthening effect on inclusions near the surface compared to the inclusions located deeper in the volume, thus shifting the crack initiation site further into the volume. Possibly, the plastic deformation during the TMT is more pronounced in near-surface regions because the respective grains have no neighboring grains in the direction to the surface. It could also be that a radial temperature gradient in the specimen's gauge length occurred during the TMT. The TMT temperature of 265 °C was reached by inductive heating and was measured and controlled at the specimen surface. The soaking time at 265 °C before the mechanical loading starts is only 15 s in order to minimize purely thermal effects. Hence, it is possible that the specimens were not completely heated through when the mechanical loading began. If the temperature in the specimen center would be significantly lower, the strengthening DSA effects might be less effective. If that were the case, an even better increase in the fatigue lifetime and fatigue strength might be possible with a more homogeneous temperature distribution in the treated volume. This may be reached with a longer soaking time at the TMT temperature before the mechanical loading begins. Figure 10 also indicates the fisheye surface structure showing that, for fisheye radii below 300 µm, the fisheye surface has only a smooth structure, while for radii above 300 µm, a smooth and a rougher, wavy structure as in Figure 9c could be observed. This is true for both TMT and HT specimens. With increasing fisheye radius, the roughness and waviness of the fracture surface becomes more pronounced. The transition from smooth to the rough fisheye structure occurred always at a radius of about 300 µm. The corresponding stress intensity factor according to Equation (1) is about 15.8 MPa.m$^{1/2}$, which may be identified as the transition stress

intensity factor to the Paris regime [10]. Obviously, if the fisheye reaches the surface before this value is reached, only a smooth fisheye structure is formed. Hence, it depends mainly on the inclusion depth whether a fisheye grows in one or two stages. The results indicate that the TMT has no influence on the fisheye formation and thus on the crack propagation. This was expected since the TMT is supposed to strengthen the microstructure very close to the inclusions and not in the bulk.

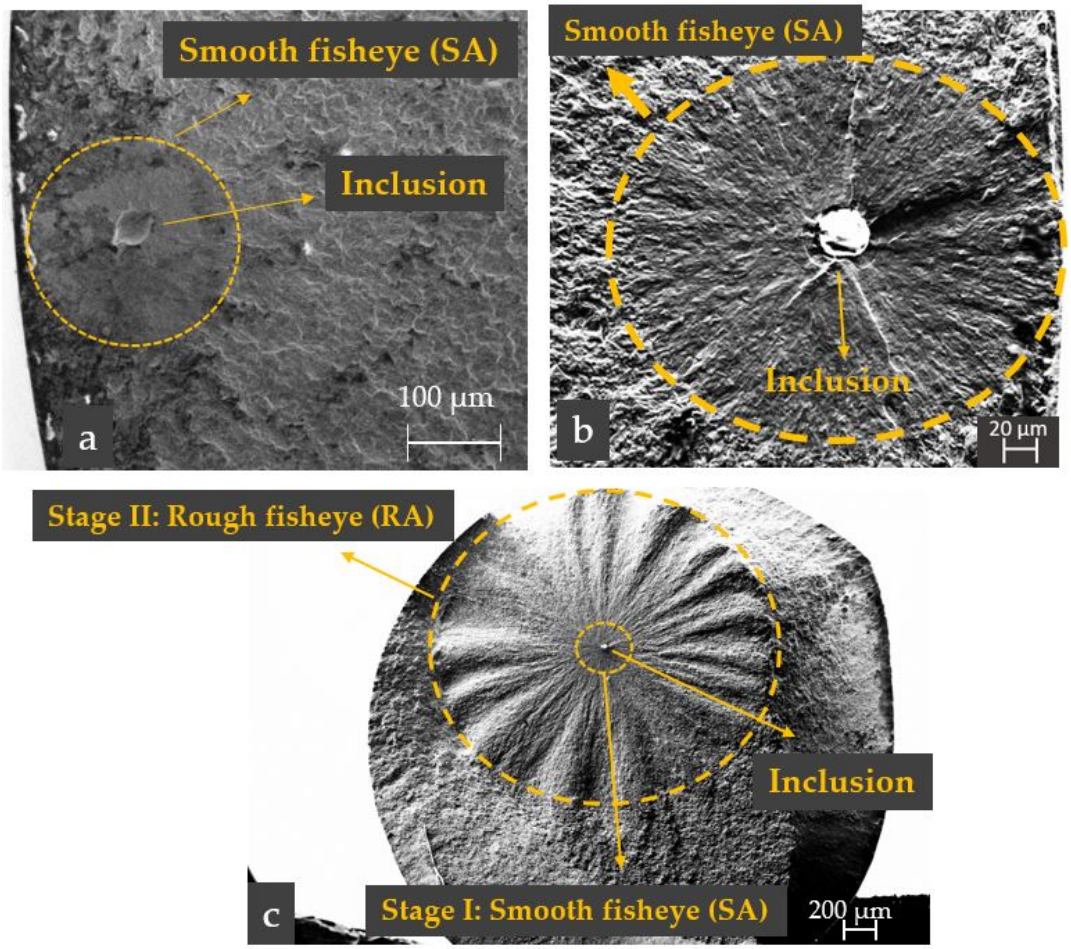

Figure 9. Fisheye formation analysis of fracture surfaces at a stress amplitude of 775 MPa. (**a**) TMT specimen, inclusion is surrounded by a smooth fisheye (fisheye formation in a single stage, N_f = 4,932,070 cycles, inclusion depth = 125 µm); (**b**) HT specimen, inclusion is surrounded by a smooth fisheye (fisheye formation in a single stage, N_f = 6,722,705 cycles, inclusion depth = 180.8 µm); (**c**) TMT specimen, inclusion is surrounded by a small smooth fisheye around the inclusion and a bigger rough fisheye around the smooth one (fisheye formation in two stages, N_f = 9,706,545 cycles, inclusion depth = 1.3 mm).

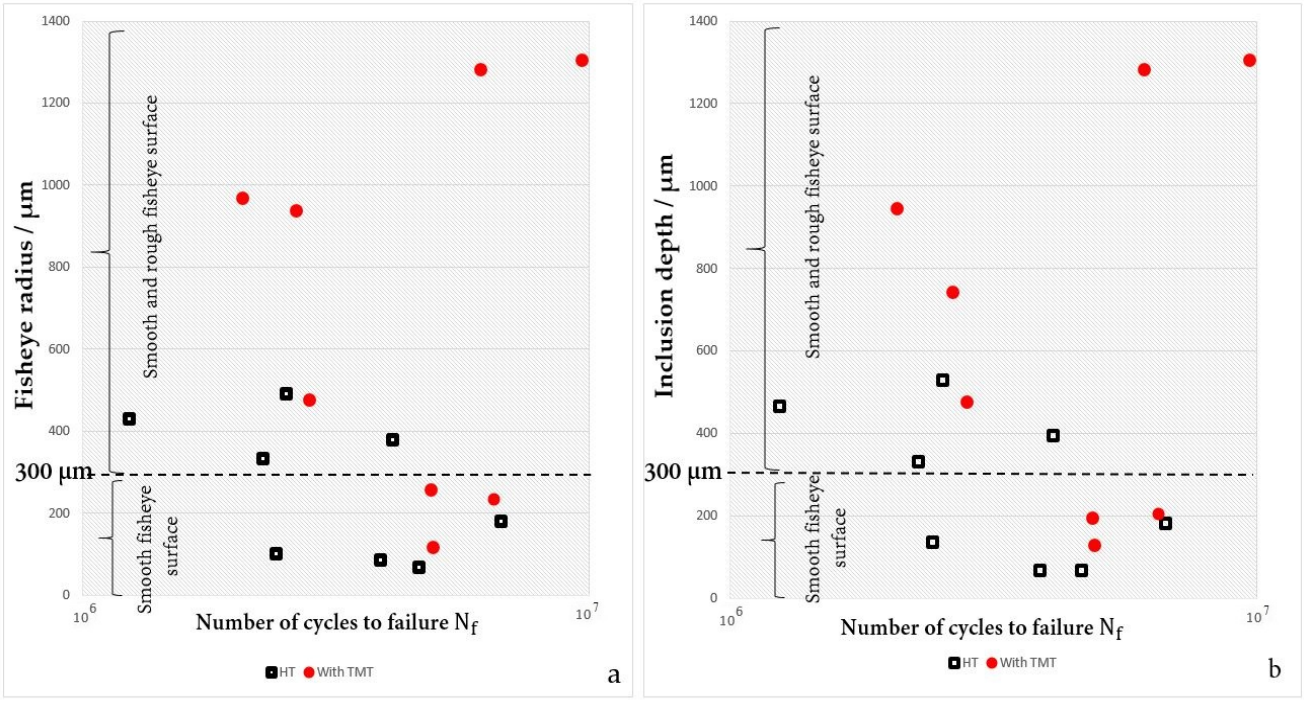

Figure 10. (**a**) Fisheye radius versus lifetime at σ_a = 775 MPa. (**b**) Inclusion depth versus lifetime at σ_a = 775 MPa.

4. Conclusions

In this study the influence of thermo-mechanical treatment (TMT) on the lifetime, internal crack initiation and crack propagation behavior under high cycle fatigue loading at a constant stress amplitude of 775 MPa was investigated. The results can be summarized as follows:

(1) For the tested stress amplitude, all specimens fractured from cracks that initiated at oxide inclusions of type AlCaO within the volume. Fisheye fracture surfaces could be observed in all cases. As expected, the TMT increased the average fatigue lifetime by about 40% due to plastic deformation in the temperature regime of dynamic strain aging, which leads to a strengthened dislocation structure around inclusions and delays crack initiation.

(2) The area of the critical inclusion and the inclusion depth has only an insignificant influence on the overall fatigue lifetime for both the TMT and HT specimens. Depending on the shape of critical inclusion, the minimum required inclusion area for the crack initiation and its corresponding stress intensity factor could change.

(3) The inclusion depth correlates strongly with the fisheye radius. This means internal cracks grow in fisheye mode until they reach the surface. When the fisheye reaches a radius of about 300 µm, which corresponds to a stress intensity factor of about 15.8 MPa.m$^{1/2}$, the fracture surface appearance changes from smooth to a rougher wavy form, which is presumably the transition to crack propagation in the Paris regime. TMT had no influence on this behavior.

(4) The TMT increases the average depth of critical inclusions considerably indicating that the strengthening of the microstructure is more effective in the near-surface regions. The reason for this might be that there is a radial temperature gradient in the specimen during the TMT resulting in varying effectiveness of dynamic strain aging effects. With a more homogeneous temperature distribution, an even better effect of the TMT might be possible.

Author Contributions: Conceptualization, A.K. and S.G.; investigation, A.K.; original draft preparation, A.K.; writing—review and editing, S.G. and M.H.; supervision, M.H. All authors have read and agreed to the published version of the manuscript.

Funding: This research project was funded by the Deutsche Forschungsgemeinschaft (DFG, German Research Foundation)—Project number 408139037.

Data Availability Statement: Not applicable.

Acknowledgments: We gratefully acknowledge the financial support by the KIT-Publication Fund of the Karlsruhe Institute of Technology.

Conflicts of Interest: There are no conflicts of interest regarding the presented work.

References

1. Murakami, Y.; Kodamab, S.; Konumac, S. Quantitative Evaluation of Effects of Non-Metallic Inclusions on Fatigue Strength of High Strength Steels. I: Basic Fatigue Mechanism and Evaluation of Correlation between the Fatigue Fracture Stress and the Size and Location of Non-Metallic Inclusions. *Int. J. Fatigue* **1989**, *11*, 291–298. [CrossRef]
2. Kucharski, P.; Lesiuk, G.; Szata, M. *Description of Fatigue Crack Growth in Steel Structural Components Using Energy Approach—Influence of the Microstructure on the FCGR*; AIP Publishing LLC: Fojutowo, Poland, 2016; p. 050003.
3. Starke, P.; Walther, F.; Eifler, D. Fatigue Assessment and Fatigue Life Calculation of Quenched and Tempered SAE 4140 Steel Based on Stress–Strain Hysteresis, Temperature and Electrical Resistance Measurements. *Fatigue Fract. Eng. Mater. Struct.* **2007**, *30*, 1044–1051. [CrossRef]
4. Mughrabi, H. On 'Multi-Stage' Fatigue Life Diagrams and the Relevant Life-Controlling Mechanisms in Ultrahigh-Cycle Fatigue: ON 'MULTI-STAGE' FATIGUE LIFE DIAGRAMS. *Fatigue Fract. Eng. Mater. Struct.* **2002**, *25*, 755–764. [CrossRef]
5. Mughrabi, H. Specific Features and Mechanisms of Fatigue in the Ultrahigh-Cycle Regime. *Int. J. Fatigue* **2006**, *28*, 1501–1508. [CrossRef]
6. Lipiński, T.; Wach, A.; Detyna, E. Influence of Large Non-Metallic Inclusions on Bending Fatigue Strength Hardened and Tempered Steels. *Adv. Mater. Sci.* **2015**, *15*, 33–40. [CrossRef]
7. Li, W.; Deng, H.; Liu, P. Interior Fracture Mechanism Analysis and Fatigue Life Prediction of Surface-Hardened Gear Steel under Axial Loading. *Materials* **2016**, *9*, 843. [CrossRef] [PubMed]
8. Shiozawa, K.; Lu, L.; Ishihara, S. S-N Curve Characteristics and Subsurface Crack Initiation Behaviour in Ultra-Long Life Fatigue of a High Carbon-Chromium Bearing Steel: S-N Curve and Crack Initiation in Ultra-Long Life Fatigue. *Fatigue Fract. Eng. Mater. Struct.* **2001**, *24*, 781–790. [CrossRef]
9. Shiozawa, K.; Murai, M.; Shimatani, Y.; Yoshimoto, T. Transition of Fatigue Failure Mode of Ni–Cr–Mo Low-Alloy Steel in Very High Cycle Regime. *Int. J. Fatigue* **2010**, *32*, 541–550. [CrossRef]
10. Stanzl-Tschegg, S.E. Fracture Mechanical Characterization of the Initiation and Growth of Interior Fatigue Cracks: Fracture Mechanics for Interior Fatigue Cracks. *Fatigue Fract. Eng. Mater. Struct.* **2017**, *40*, 1741–1751. [CrossRef]
11. Stanzl-Tschegg, S.; Schönbauer, B. Near-Threshold Fatigue Crack Propagation and Internal Cracks in Steel. *Procedia Eng.* **2010**, *2*, 1547–1555. [CrossRef]
12. Li, Y.-D.; Zhang, L.-L.; Fei, Y.-H.; Liu, X.-Y.; Li, M.-X. On the Formation Mechanisms of Fine Granular Area (FGA) on the Fracture Surface for High Strength Steels in the VHCF Regime. *Int. J. Fatigue* **2016**, *82*, 402–410. [CrossRef]
13. Guo, J.; Han, S.; Chen, X.; Guo, H.; Yan, Y. Control of Non-Metallic Inclusion Plasticity and Steel Cleanliness for Ultrathin 18 Pct Cr-8 Pct Ni Stainless Steel Strip. *Metall. Mater. Trans. B* **2020**, *51*, 1813–1823. [CrossRef]
14. Yang, Z.G.; Li, S.X.; Zhang, J.M.; Zhang, J.F.; Li, G.Y.; Li, Z.B.; Hui, W.J.; Weng, Y.Q. The Fatigue Behaviors of Zero-Inclusion and Commercial 42CrMo Steels in the Super-Long Fatigue Life Regime. *Acta Mater.* **2004**, *52*, 5235–5241. [CrossRef]
15. Xie, J.P.; Wang, A.Q.; Wang, W.Y.; Li, J.W.; Yang, D.X.; Zhang, K.F.; Ma, D.Q. Stress Field Numerical Simulation of the Inclusions in Large Rudder Arm Steel Casting. *Adv. Mater. Res.* **2011**, *311–313*, 906–909. [CrossRef]
16. Gu, C.; Liu, W.; Lian, J.; Bao, Y. In-Depth Analysis of the Fatigue Mechanism Induced by Inclusions for High-Strength Bearing Steels. *Int. J. Miner. Metall. Mater.* **2021**, *28*, 826–834. [CrossRef]
17. da Costa e Silva, A.L.V. The Effects of Non-Metallic Inclusions on Properties Relevant to the Performance of Steel in Structural and Mechanical Applications. *J. Mater. Res. Technol.* **2019**, *8*, 2408–2422. [CrossRef]
18. Krewerth, D.; Lippmann, T.; Weidner, A.; Biermann, H. Influence of Non-Metallic Inclusions on Fatigue Life in the Very High Cycle Fatigue Regime. *Int. J. Fatigue* **2016**, *84*, 40–52. [CrossRef]
19. Murakami, Y.; Endo, M. Effects of Defects, Inclusions and Inhomogeneities on Fatigue Strength. *Int. J. Fatigue* **1994**, *16*, 163–182. [CrossRef]
20. Kerscher, E.; Lang, K.; Vohringer, O.; Lohe, D. Increasing the Fatigue Limit of a Bearing Steel by Dynamic Strain Ageing. *Int. J. Fatigue* **2008**, *30*, 1838–1842. [CrossRef]
21. Kerscher, E.; Lang, K.-H.; Löhe, D. Increasing the Fatigue Limit of a High-Strength Bearing Steel by Thermomechanical Treatment. *Mater. Sci. Eng. A* **2008**, *483–484*, 415–417. [CrossRef]

22. Khayatzadeh, A.; Sippel, J.; Guth, S.; Lang, K.-H.; Kerscher, E. Influence of a Thermo-Mechanical Treatment on the Fatigue Lifetime and Crack Initiation Behavior of a Quenched and Tempered Steel. *Metals* **2022**, *12*, 204. [CrossRef]
23. Guan, J.; Wang, L.; Zhang, C.; Ma, X. Effects of Non-Metallic Inclusions on the Crack Propagation in Bearing Steel. *Tribol. Int.* **2017**, *106*, 123–131. [CrossRef]
24. Shiozawa, K.; Hasegawa, T.; Kashiwagi, Y.; Lu, L. Very High Cycle Fatigue Properties of Bearing Steel under Axial Loading Condition. *Int. J. Fatigue* **2009**, *31*, 880–888. [CrossRef]
25. Liu, P.; Li, W.; Nehila, A.; Sun, Z.; Deng, H. High Cycle Fatigue Property of Carburized 20Cr Gear Steel under Axial Loading. *Metals* **2016**, *6*, 246. [CrossRef]
26. Lei, Z.; Hong, Y.; Xie, J.; Sun, C.; Zhao, A. Effects of Inclusion Size and Location on Very-High-Cycle Fatigue Behavior for High Strength Steels. *Mater. Sci. Eng. A* **2012**, *558*, 234–241. [CrossRef]
27. Taheri, F.; Trask, D.; Pegg, N. Experimental and Analytical Investigation of Fatigue Characteristics of 350WT Steel under Constant and Variable Amplitude Loadings. *Mar. Struct.* **2003**, *16*, 69–91. [CrossRef]
28. Labisch, S.; Weber, C. *Technisches Zeichnen*; Springer: Wiesbaden, Germany, 2014; ISBN 978-3-8348-0915-5.
29. Kaiser, D. *Experimentelle Untersuchung und Simulation des Kurzzeitanlassens unter Berücksichtigung Thermisch Randschichtgehärteter Zustände am Beispiel von 42CrMo4*; Karlsruher Institut für Technologie: Karlsruhe, Germany, 2019; p. 194.
30. Lang, K.-H.; Korn, M.; Rohm, T. Very High Cycle Fatigue Resistance of the Low Alloyed Steel 42CrMo4 in Medium- and High-Strength Quenched and Tempered Condition. *Procedia Struct. Integr.* **2016**, *2*, 1133–1142. [CrossRef]